2.25 Auditory Afferents: Sound Encoding in the Cochlea

Sonja J Pyott[a] **and Henrique von Gersdorff**[b], [a] University of Groningen, University Medical Center Groningen, Department of Otorhinolaryngology and Head/Neck Surgery, Groningen, the Netherlands; and [b] The Vollum Institute, Oregon Health and Science University, Portland, OR, United States

2.25.1 Abstract

Sounds and moments of silence inform and enrich our world. They convey critical information for the survival and social prospering of animals. The great diversity of acoustic signals in the natural world, from soft and transient to loud and prolonged sounds over a range of frequencies, needs to be detected, encoded, and transmitted continuously to the brain. Accordingly, recent advances in understanding the biology of the primary auditory neurons, which are tasked with this challenge, reveal a great heterogeneity in their morphology, physiology, and patterns of protein and gene expression. This heterogeneity is essential to providing diverse ascending relay pathways for the encoding and transmission of different streams of acoustic information. However, it also unfortunately provides a substrate for axonal vulnerability and hearing loss. This chapter outlines the mechanisms by which auditory neurons perform the remarkable feat of precise sound encoding and also the factors that contribute to their heterogeneity.

2.25.2 Afferent Fiber Heterogeneity is Essential to Relay Diverse Acoustic Information to the Brain

Complex and rapidly changing sounds impinging on the tympanic membrane eventually lead to displacements of stereocilia bundles on the apical pole of the inner hair cells (IHCs) within the cochlea (**Fig. 1**A). Soft sounds produce minute movements of the stereocilia, whereas louder sounds produce larger displacements. The opening and closing of mechanically gated ion channels in the lower stereocilia tips lead to changes in the IHC membrane potential (an analog signal) that eventually trigger action potential spikes (a digital, all-or-none signal) in the auditory nerve, the eighth (VIII) cranial nerve of mammals. The auditory nerve is one of the shortest nerves of mammals, so signals arrive to the brain (specifically to the cochlear nucleus) with short temporal delays. The analog-to-digital conversion of sound signals (mechanical energy) in the inner ear to action potential discharges (spikes) in the auditory nerve occurs in part via the release of glutamate onto afferent fiber boutons (approximately 0.5–3 μm in diameter) at ribbon synapses in the basal pole of the IHC (**Fig. 1**A; Liberman, 2017; Moser et al., 2020).

In mammals, a single IHC is contacted by 10–15 afferent fibers, with each fiber arising from a single auditory neuron and contacting one synaptic ribbon (Rutherford and Moser, 2016; Coate et al., 2019). However, some rare afferent fibers may be contacted by two or three closely-spaced ribbons. Synaptic ribbons mark the sites of glutamate release and Ca^{2+} channel clustering in the IHC and are opposed to AMPA receptor clusters in the postsynaptic density of the afferent fiber bouton terminals (Rutherford, 2015). **Fig. 1**A shows that there are two main types of fibers that contact different parts of the IHC, the mediolar and pillar sides of the IHC. The afferent fibers originate from the primary auditory neurons—the spiral ganglion neurons (SGNs)—as a thin dendrite that becomes myelinated by Schwann cells. The SGNs show great diversity in their abundance, morphology, and physiology. The Type I and type II SGNs differ most conspicuously from one another in their myelinization, caliber, relative number, and synaptic connections. Type I SGNs, which are the principle sensory neurons, have a myelinated soma in cats, but not humans. Their axons have relatively large diameters, and comprise approximately 95% of the total SGN axonal population. They receive synaptic input from a single IHC. In contrast, type II SGNs are unmyelinated, much smaller in caliber, and comprise the remaining 5% of the SGN population. They receive input from multiple outer hair cells (OHCs; see **Fig. 2**; Muniak et al., 2016) and their function is not yet completely clear, although it is hypothesized that they transmit pain information evoked by loud sounds to the CNS (Fuchs, 2018). In addition, they may relay the depolarized state of the OHCs to the brainstem and thus help to tune the efferent fibers from the

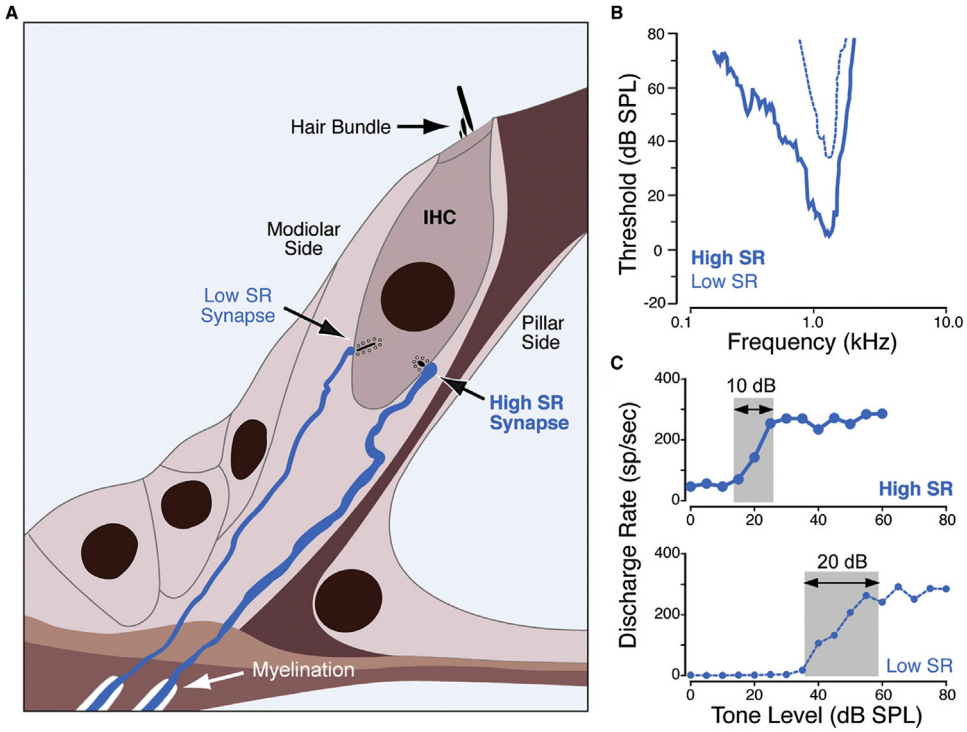

Figure 1 The Inner Hair Cell (IHC) and Its Synaptic Connections to Afferents. (A) Two types of afferents are found connected to the same IHC: a high spontaneous rate (high SR) fiber on the pilar side of the IHC and a low spontaneous rate (low SR) fiber on the mediolar side of the IHC. Note the thin diameter of the low SR fiber that is connected to a large synaptic ribbon (the site of synaptic vesicle fusion and glutamate release) and the thick diameter of the high SR fiber that is connected to a small synaptic ribbon. (B) Tuning curves for high SR fibers have a low threshold (these fibers have a high sensitivity to soft sounds), whereas low SR fibers have a high threshold (these fibers are less sensitive of soft sounds). (C) Discharge rates (spikes per second) of high SR fibers and low SR fibers. Note that even in silence (0 dB SPL) the high SR fiber spikes at 50 Hz. High SR fibers have a smaller dynamic range (gray area) before they saturate at 300 Hz than low SR fibers. Modified from Liberman (2017).

brainstem that make cholinergic synapses on the OHCs. A type II afferent-to-efferent feedback loop may thus modulate the overall gain of the cochlear amplifier (Muniak et al., 2016; Vattino et al., 2020).

The type I SGNs have been classified based on their physiological properties, most notably their low or high sound threshold sensitivity and their spontaneous firing rates. As shown in **Fig. 1**A, a low threshold peripheral fiber has a thick axon caliber (1.3–1.8 μm in cat; Tsuji and Liberman, 1997) and tends to have a high spontaneous rate (**Fig. 1**B and 1C). It forms synapses with a small presynaptic ribbon and a large postsynaptic density on the pillar side of the IHC. The large axon contains multiple mitochondria along its length, presumably to provide metabolic support for high frequency firing. The spike propagation velocity will also be faster in larger caliber axons. By contrast, a high threshold fiber has a thin axon caliber (0.8–1.0 μm in cat; Tsuji and Liberman, 1997) and tends to have a low spontaneous rate (**Fig. 1**A and B). It forms synapses with a relatively large presynaptic ribbon and a small postsynaptic density on the modiolar side of the IHC. The spike propagation velocity will presumably be slower in these thin caliber axons, although the axon caliber increases as the SGN axons form the auditory nerve.

A single IHC, depolarized by an acoustic signal, thus sends parallel streams of spikes at different rates and velocities via 10 to 15 distinct information relays (the afferent fibers). Information from soft sounds (low threshold) is sent via high spontaneous rate fibers that have a small dynamic range in intensity (~10 dB; **Fig. 1**C), whereas louder sounds (high threshold) are sent via low spontaneous rate fibers that have a larger dynamic range in intensity (approximately 20 DB; **Fig. 1**C). The quick saturation of discharge rate (spikes/seconds) over a short range (approximately 10 dB) suggests that high spontaneous rate fibers may have a more depolarized resting membrane potential (V_m (rest)) and/or a lower spike membrane voltage threshold than low spontaneous rate fibers. This hypothesis of a more depolarized V_m (rest) would also explain how small current injections (via small spontaneous mEPSC) may lead to higher spontaneous rate spikes. By contrast, low spontaneous rate fibers may have a more hyperpolarized V_m (rest) and/or higher spike threshold, perhaps due to a larger expression of voltage-gated K^+ channels (causing a lower V_m (rest) and a smaller expression of voltage-gated Na^+ channels (causing a higher spike threshold). In addition, differences in the presynaptic IHC voltage-dependent Ca^{2+} current activation curves and the number of Ca^{2+} channels may also contribute to differences in low to high spontaneous rate spikes from fibers connected to a single IHC (Ohn et al., 2016). The small ribbons of high spontaneous rate synapses may have a larger density of high open probability Ca^{2+} channels that trigger exocytosis even at more hyperpolarized potentials via nanodomain coupling to docked vesicles. Whereas the larger ribbons of low spontaneous rate synapses may have a larger density of low open probability Ca^{2+} channels that may open cooperatively to trigger multivesicular exocytosis only at more depolarized potentials (Rodriguez-Contreras and Yamoah, 2001; Li et al., 2009; Graydon et al., 2011; Zampini et al., 2010).

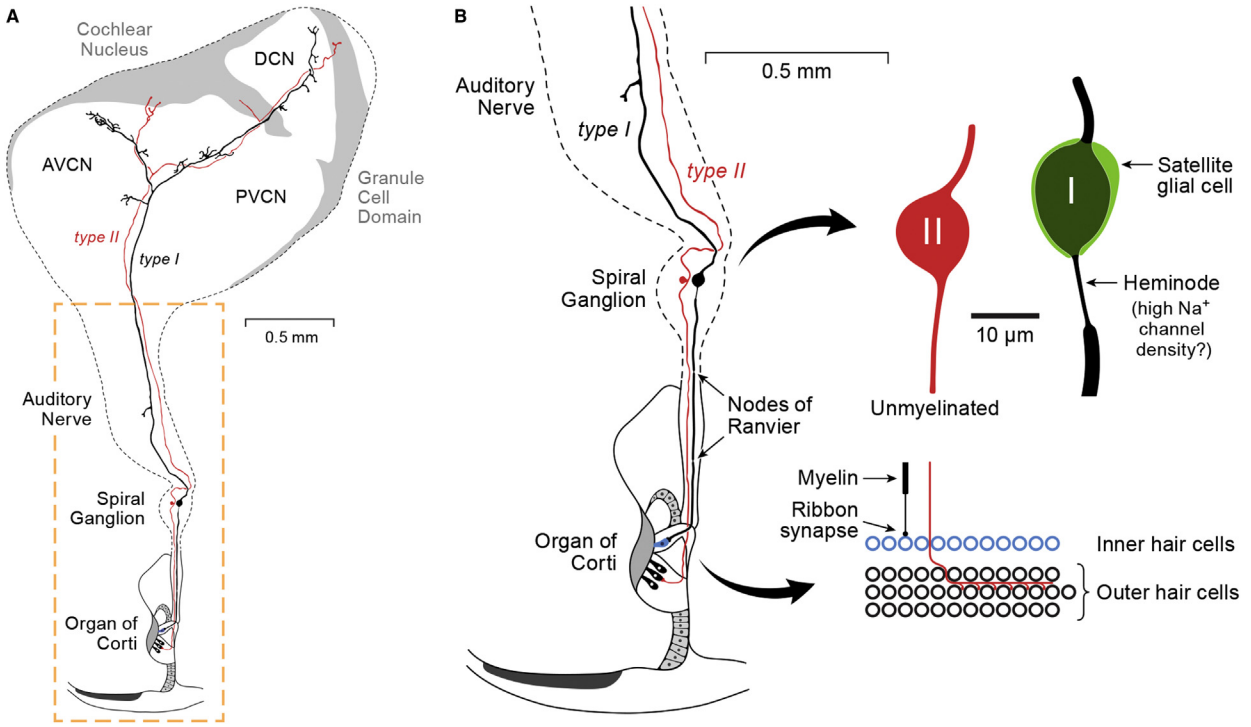

Figure 2 The Spiral Ganglion Neurons (SGNs) and Their Synaptic Connections Within the Cochlea and the Cochlear Nucleus (CN) of Cat. (A) The Type I afferent connects to a single IHC, whereas the Type II afferent connects to multiple outer hair cells (OHCs). Type I and Type II afferents send projections to the anterior ventral cochlear nucleus (AVCN), the posterior ventral cochlear nucleus (AVCN) and the dorsal cochlear nucleus (DCN). The granule cell domain is shown in gray. (B) This is an expanded view of the dashed rectangle area in panel (A) The organ of Corti contains a single row of IHCs (blue) and three rows of outer hair cells (OHC). Note the relatively thick axon caliber and myelination of the Type I fiber, whereas the Type II has a thin caliber axon that is not myelinated. The Type I cell soma is surrounded by a thin satellite glia cell (green), which may reduce its membrane capacitance. In cat there are two nodes of Ranvier and three internode myelin segments before reaching the Type 1 spiral ganglion neuron (SGN) soma. The Type I afferent axon becomes more narrow as it approaches the soma and this may be a region of high Na^+ channel density. This is the peripheral afferent. After the spiral ganglion soma there are about 12 (or less) internodal segments before the central afferent terminates in a presynaptic terminal in the cochlear nucleus (Liberman and Oliver, 1984). Note the relatively short length of the auditory (eighth) nerve, which is the shortest nerve in the mammalian CNS. Modified from Muniak et al. (2016).

All aspects of acoustic signals, namely, their frequency, intensity, onset and offset must be rapidly and precisely encoded via spikes in different auditory nerve axons. For humans, the dynamic range of frequency varies from 20 Hz to 20 kHz, whereas the range of intensity spans 6 orders of magnitude in sound pressure (or from 0 to 120 dB). However, this large bandwidth of information must be compressed because spike trains along the axons have frequencies that vary over only 2 orders of magnitude; namely from zero to about 300 Hz (**Fig. 1**C). The multiplexing to 10 to 15 fibers, each with a different spike timing and rate, allows a single IHC to increase its bandwidth of output signals.

The human cochlea has only approximately 3500 IHCs located on top of the basilar membrane (30–35 mm in spiral length and 2.75 cochlear turns) that connect to approximately 40,000 Type I SGN fibers that will form the auditory nerve. By comparison, the human retina has approximately 100 million photoreceptors and 1 million optic nerve fibers. Therefore, it appears that to build an accurate representation of the visual and acoustic world the mammalian CNS requires ~100-fold more optic nerve fibers than the auditory nerve fibers. In contrast to humans, the gerbil, a rodent with good low frequency hearing, has about ~1560 IHCs located on top of its basilar membrane (11–12.7 mm in spiral length and 2.5 cochlear turns; Risoud et al., 2017), whereas the mouse, a rodent with poor hearing below 1–2 kHz, has only about ~765 IHCs located on top of its basilar membrane (5–6 mm in spiral length and 2 cochlear turns; Burda and Branis, 1988). It appears that in the evolutionary niche of the mouse the extra energetic expense of low frequency hearing was not imperative for survival.

The physiological heterogeneity of the type I SGNs thus provides nonredundant, parallel streams of auditory information to the brain that is essential to encode the large dynamic range and spectral complexity of auditory stimuli. Moreover, this heterogeneity correlates with the susceptibility to loss of SGNs in acquired hearing loss (see Section "**Auditory Synaptopathy and Hidden Hearing Loss**") and recent work shows that loss of subpopulations of SGNs affects central auditory structures. Although much less studied, type II SGNs show very different physiological properties from the type I SGNs (Fuchs, 2018). The type II SGN fibers are unmyelinated and have a small caliber (0.1–1 µm; Arnesen and Osen, 1978, **Fig. 2**). The lack of myelination and thinner caliber, will lead presumably to slow spike propagation, analogous to dorsal root ganglion C-fibers that carry pain, itch and heat information (Fuchs, 2018). Type II SGN fibers receive synaptic input from multiple OHCs, but have poor acoustic sensitivity and a high sound threshold for spiking, whereas Type I receive input from one IHC and vary in threshold (Fuchs, 2018). Type II fibers probably spike at very low rates, given they small caliber, and accordingly, do not express the Na/K-ATPase α3 pump protein, which is strongly

expressed in the Type I fiber (McLean et al., 2009). Although the physiological heterogeneity between type I and type II SGNs, and among subpopulations of type I SGNs, is well documented, the molecular mechanisms and ion channel characteristics underlying this heterogeneity are far from understood (but see Section "**Transcriptomic Insights into the Determinants of Afferent Neuron Heterogeneity**" below).

2.25.3 The Encoding of Sound Frequency and Intensity

The particular frequency of a sound is detected and encoded by a base-to-apex tonotopic map within the cochlea: low frequency sounds are encoded by auditory neurons that synapse with IHCs in the apex of the cochlea and high frequency sounds are encoded by auditory neurons from the base of the cochlea (**Fig. 3**; Muniak et al., 2016). This tonotopic arrangement creates a labeled line code of frequency. The mechanical tuning properties of the mammalian basilar membrane form the basis for this frequency selectivity of the auditory fibers. **Fig. 1**B shows the sharp tuning curve to two different afferents that are tuned to the same frequency (approximately 1.5 kHz) although one is a high spontaneous rate (low threshold) fiber and the other a low spontaneous rate (high threshold) fiber. These afferents thus receive synaptic inputs from nearby IHCs or can even be connected to the same IHC.

The apex-to-base tonotopic map of the cochlea, representing the low to high frequency sound signals, respectively, is transferred and preserved in the outputs afferents fibers that emanate from the SGNs and synapse onto the neurons of the cochlear nucleus (CN). The nerve endings of these afferents are thus organized along a tonotopic map in the anterior ventral cochlear nucleus (aVCN) and dorsal cochlear nucleus (DCN; **Figs. 2** and **3**). Note the logarithmic-like distribution of sound frequencies in the aVCN and DCN (**Fig. 3**).

Afferent axons contacting IHCs in the peripheral are myelinated by Swann cells, whereas they are myelinated by oligodendrocytes after they leave the spiral ganglion and form the VIII cranial nerve, a CNS nerve. The cat afferent fiber that contacts the IHC has 2 nodes of Ranvier before it reaches the SGN soma and the internode segment is ~200 μm in length (**Fig. 2**; Liberman and Oliver, 1984). The axon then has ~12 nodes of Ranvier as it projects from the SGN soma to the nerve terminal in cochlear nucleus and the internode segment increases in length ~200–400 μm (Liberman and Oliver, 1984). Cutting a slice through the cat auditory nerve one observes that the central core of the axon fascicle has fibers that tend to have low characteristic frequency (CF; the frequency requiring the lowest sound pressure level (SPL) for spike rate increases) and larger diameters (3.6–4.2 μm), whereas the shell (outer) region has higher CF and smaller diameters (2.8–3.2 μm; Arnesen and Osen, 1978). However, a similar analysis in the guinea pig

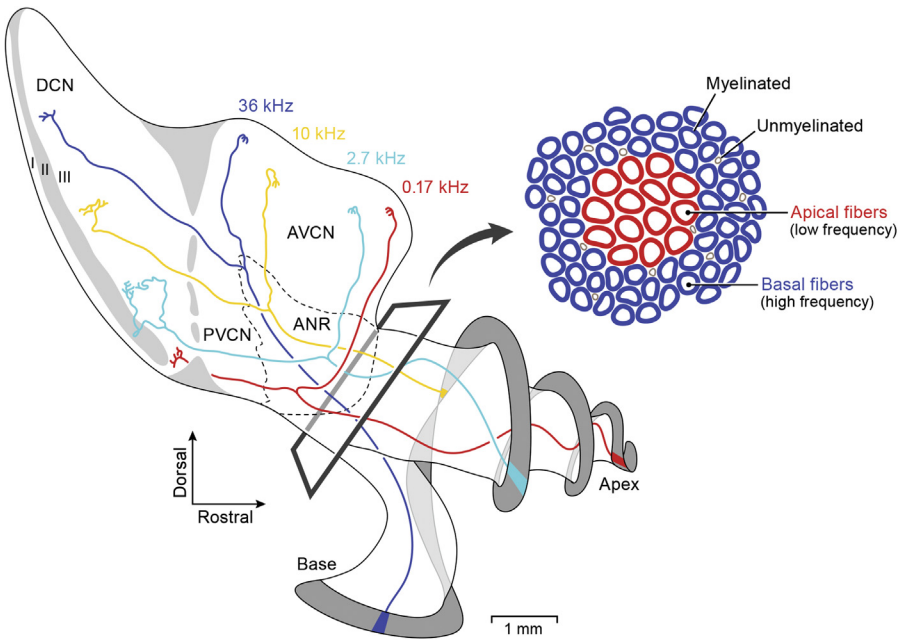

Figure 3 **The Tonotopic Map of the Cochlea and Its Projections to the Cochlear Nucleus.** This diagram shows that cat cochlea and cochlear nucleus. The apex of the cochlea has IHCs and afferents that encode low sound frequencies (red), whereas the base of the cochlea has IHCs and afferents that encode high sound frequencies (blue). The red afferent has a characteristic (or best) frequency of 170 Hz and the blue afferent has a characteristic frequency of 36 kHz. The characteristic frequency is the frequency at the peak of the tuning curve (or the frequency of greatest sensitivity; see **Fig. 1**C). A rectangular slice through the auditory nerve root (ANR) reveals a fiber bundle of myelinated (Type 1) and unmyelinated fibers (Type 2). The central core of the bundle (red) has relatively large caliber axons tuned to low frequencies and the outer layer (blue) has smaller caliber axons tuned to high frequencies. The nerve endings in the anterior ventral cochlear nucleus (AVCN) are the end bulbs of Held that synapse onto the bushy cells. Modified from Muniak et al. (2016).

auditory nerve found the opposite, namely, axons derived from the basal (high CF) cochlea turn had larger diameters (4.0–4.6 μm) than the apex (low CF) cochlear turn (1.4–2.0 μm; Friede, 1984). It is possible that species with different brain sizes and hearing requirements as predators may develop different axon calibers and myelination along the auditory nerve.

Afferents with a low characteristic frequency (<2 kHz) can also encode sound frequency via phase-locked spikes (a spike time code). This feature of the auditory nerve is crucial for the localization of low-frequency sound sources and spatial hearing by the brain (Grothe and Pecka, 2014). Auditory nerve fibers (ANFs) in frog, turtles and birds also express heterogeneous spike rates and contact many synaptic ribbons, a feature that may increase their dynamic range and sensitivity to soft sounds if different ribbons in the same hair cell have different Ca^{2+} channel clusters and release probability (Rodriguez-Contreras and Yamoah, 2001; Graydon et al., 2014; Schnee et al., 2013; Chen and von Gersdorff, 2019). **Fig. 4**A shows a paired recording from a single bullfrog auditory hair cell and a connected afferent fiber. Note that the afferent fiber action potential spikes occur at a precise time during the 400 Hz stimulus sine wave cycle (Li et al., 2014). Note also that many spontaneous and evoked excitatory postsynaptic potentials (EPSPs) do not reach the threshold to trigger a spike (Schnee et al., 2013; Li et al., 2014). At mammalian afferent fibers small EPSCs can trigger a spike in the high input resistance afferent (Rutherford et al., 2012), however some EPSCs do not reach spike threshold and afferents can also spike spontaneously in the absence of EPSCs (Wu et al., 2016).

Mammalian ANFs can fire a spike within a precise phase (or time) or the sine wave cycle of a pure tone sound wave (**Fig. 4**B; Goutman, 2012; Heil and Petersen, 2017). If one considers the unmyelinated portion of the ANF as having a resting membrane capacitance (C_m) of about 2 pF and a membrane time constant $\tau = 1$ ms this produces an input membrane resistance ($\tau = R_m{*}C_m$) of about 0.5 Gohm, if one ignores cable properties, which will tend to speed the EPSP decay. An EPSC with amplitude I = 100 pA, for example, would then generate a depolarization of 50 mV ($\Delta V = R_m{*}I$), likely sufficient for passive transmission along the axon cable and spike threshold at the spike triggering heminode region (Kim and Rutherford, 2016). An ANF with these passive properties and EPSC amplitudes would thus, in principal, be able to spike at 300 Hz (**Fig. 1**C). Accordingly, more mature rat ANFs have EPSC amplitude distributions with a Gaussian peak at 300 pA and amplitudes of up to 800 pA (Grant et al., 2010). Such large

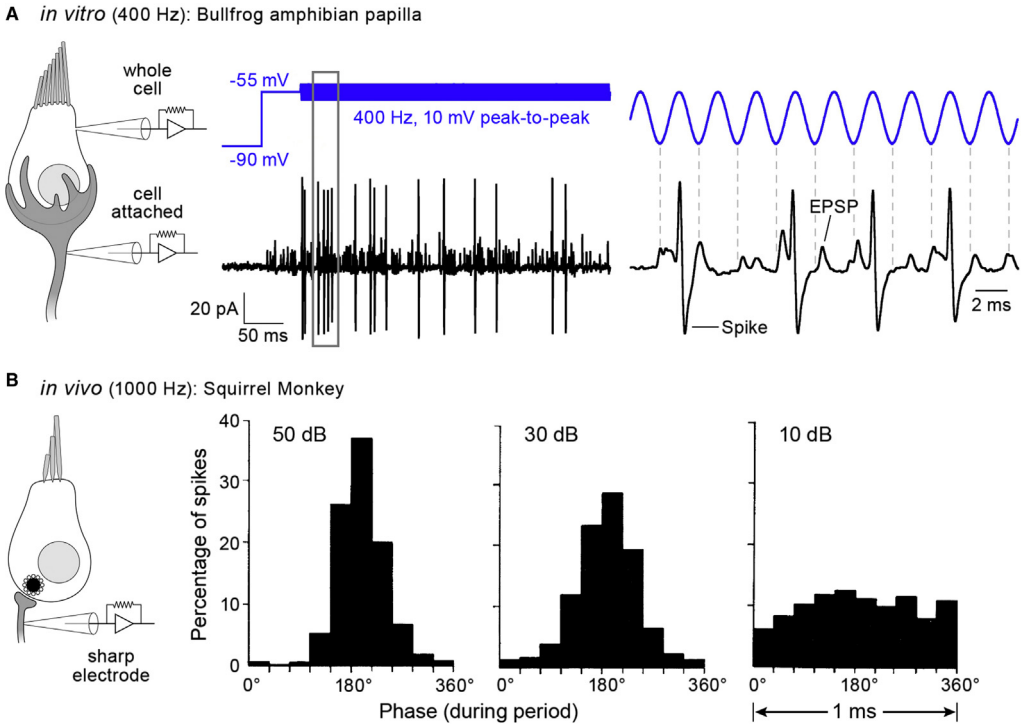

Figure 4 **Auditory Afferent Fiber Recordings: Phase-locking at Different Sound Intensities.** Paired recording from the bullfrog amphibian papilla. (A) Whole cell voltage-clamp recording from the hair cell, which was held at −90 mV and then at −55 mV, a potential close to the *in vivo* resting potential of a hair cell in silence. A sinewave voltage command (400 Hz; 10 mV peak-to-peak amplitude) was then applied to the hair cell (blue trace). A second patch pipette in the cell attached mode records simultaneously spikes and smaller "spikelets" (EPSPs) that do not reach threshold. The gray rectangular box area is shown in greater time resolution at the right panel. Note that every spike is preceded by an EPSP and many EPSPs do not trigger a spike. Spikes occur during a preferential phase of the sine wave; a phenomenon known as phase locking. (B) Period histograms of single unit recordings from *in vivo* auditory nerve fiber of squirrel monkey. The unit had a characteristic frequency (CF) of 1 kHz and a spike rate of 46 Hz at 0 dB SPL. Spikes evoked by a 1 kHz sound occur at a particular phase (or time) of the tone stimulus for tones of different intensity (measured as dB SPL). As SPL increased by 4 orders of magnitude from 10 dB to 50 dB the spike rate increased to 150 Hz but the peak in the period histogram remained relatively unchanged near 180° (or about half way through the 1 ms period). Average response phase thus changes little while vector strength (an index of synchronization) changes from 0.2 (low synchrony) at 10 dB to 0.9 (predominantly in phase) at 50 dB. At CF, the mean response phase can remain constant, allowing phase-locking that is invariant to intensity. (A) Modified from Li et al. (2014). (B) Modified from Rose et al. (1967).

EPSCs also generate spikes with more precise timing (Rutherford et al., 2012; Li et al., 2014). Synapses with a high rate of large spontaneous EPSCs (e.g., with I > 100 pA) would thus produce high spontaneous spike rate ANFs.

Fig. 4B shows period histograms of single unit recordings from *in vivo* auditory nerve fiber of squirrel monkey. As the sound stimulus intensity is increased from 10 dB to 50 dB the peak of the period histogram remains unchanged near 180°. Note also that from 10 dB to 50 dB the spike rate increases and the vector strength (or index of synchronization) changes from 0.2 (low synchrony) at 10 dB to 0.9 (high phase-locking). At the CF, the mean response phase can thus remain constant, allowing phase-locking that is independent of sound intensity (Rose et al., 1967). This shows that the intensity of a sound is encoded by the frequency of evoked spikes: soft sounds are encoded by low spike frequencies and loud sounds by high spike frequencies (a spike frequency code). The evoked first spike latency also can encode sound intensity: short latencies for loud sounds and long latencies for soft sounds (a latency code; Wittig and Parsons, 2008; Heil and Peterson, 2017). Moreover, a brief sound composed of different frequencies and intensities will evoke spikes over several fibers originating from different cochlear locations, which in parallel encode information from that particular sound (a population code). The mechanical tuning of the basilar membrane thus produces a Fourier decomposition of the different frequency components of a complex sound. The pattern of spikes in a given set of auditory nerve axons thus encodes all aspects of a complex sound stimulus.

2.25.4 Transcriptomic Insights into the Determinants of Afferent Neuron Heterogeneity

As introduced (Section "**Afferent Fiber Heterogeneity is Essential to Relay Diverse Acoustic Information to the Brain**"), sound encoding requires SGNs with a diversity of physiological responses. Our understanding of the intrinsic heterogeneity of SGN has been revolutionized recently by work leveraging single cell whole transcriptomic sequencing to identify the molecular determinants of SGN diversity (Petitpré et al., 2018; Shrestha et al., 2018; Sun et al., 2018). Very recent work provides additional comprehensive transcriptomic analysis of SGNs isolated from mice at five developmental ages (Li et al., 2020). In this first trio of studies, subtype specification was determined using bioinformatic analysis of gene expression and patterns of co-expression among SGNs isolated from mice. The findings across studies are remarkably consistent and provide important insights into the molecular differences defining SGN subtypes as well as the developmental processes regulating subtype specification. Each of these three studies classified the SGNs into four subtypes, including three classes of type I SGNs and one class of type II SGNs. Remarkably, the classification of type I SGNs into three subtypes corresponds to earlier physiological classifications of SGNs in cats into three types based on their spontaneous rates of firing and inversely correlated thresholds (Liberman, 1978). Importantly, in the smaller mouse cochlea, which does not have a representation of frequencies below 1 kHz, differences in spontaneous rate are not as distinct as they are in cat (Taberner and Liberman, 2005).

Not surprisingly given the profound differences in the connectivity and function of type I and II SGNs, the most transcriptomic differences (including non-overlapping patterns of gene expression) were observed between the collective type I SGNs and the type

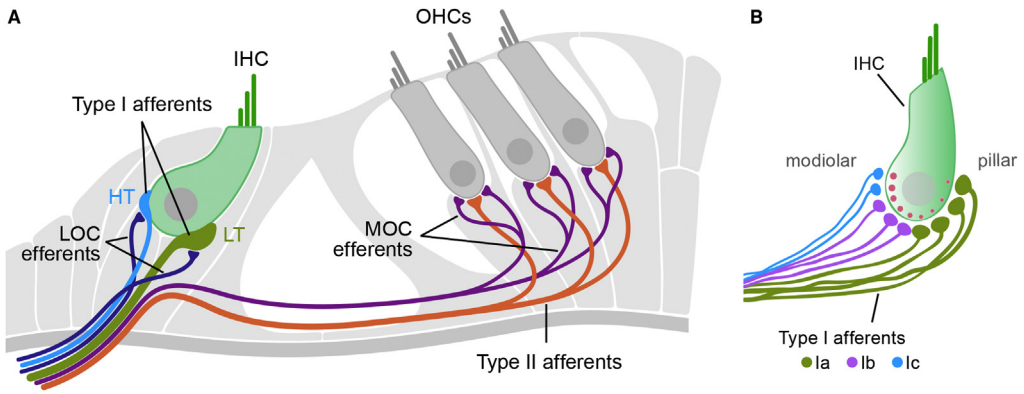

Figure 5 Organization of the Type I and Type II Spiral Ganglion Neurons (SGNs). (A) Type I SGNs contact the inner hair cells (IHCs), whereas type II SGNs contact the outer hair cells (OHCs). Type I SGNs have low (LT) or high (HT) sound thresholds. The type I and type II afferent fibers (AF type I and II) differ in their abundance, myelination, number of hair cell contacts (Section "**Afferent Fiber Heterogeneity is Essential to Relay Diverse Acoustic Information to the Brain**"), and transcriptional profiles (Section "**Transcriptomic Insights Into the Determinants of Afferent Neuron Heterogeneity**"). The type I SGNs greatly outnumber the type II SGNs, which comprise only 2%–7% of the total SGN population. Type I afferent fibers receive lateral efferent olivocochlear innervation (LOC; Section "**Lateral Efferent Innervation Modulates Afferent Neuron Activity**"). OHCs receive direct medial efferent olivocochlear innervation (MOC; this input emanates from the brainstem). (B) The type I SGNs can be subdivided based on their transcriptional profiles. The type Ia fibers comprise 35%–46% of the total SGN population and correspond to the low threshold and high spontaneous rate afferent fibers. They are transcriptionally identified by relatively high *Calb2* expression. The type Ib fibers comprise 27%–40% of the total SGN population and are transcriptionally identified by relatively high *Calb1* expression. The type Ic fibers comprise 25%–34% of the total SGN population and correspond to the high threshold and low spontaneous rate afferent fibers. They are transcriptionally identified by relatively high *Pou4f1* and *Lypd1* expression. (B) Figure modified from Shrestha et al. (2018).

II SGNs (Fig. 5A). With only slight variation between studies, these transcriptome differences identified 93% to 98% of the total SGNs as type I SGNs and 2% to 7% of the total SGNs as type II SGNs, consistent with previous histological estimations (Spoendlin, 1969; Berglund and Ryugo, 1991). Transcripts distinguishing type I and type II SGNs included *Tubb3* and *Nefl* (both encoding structural proteins), *Kcnc3* (encodes $K_V3.3$ potassium voltage-gated ion channel; promotes high-frequency spike firing), *Scn4b* (encodes Na^+ voltage-gated ion channel beta subunit 4; increases resurgent Na^+ current amplitude; promotes high-frequency spike firing), and *Prox1* (a transcription factor) in type I SGNs and *Prph* (encoding a type III intermediate filament), *Gata3* and *Mafb* (transcription factors), and *Th* (encoding tyrosine hydroxylase) in type II SGNs (Petitpré et al., 2018; Sun et al., 2018). Additional expression differences between type I and II SGNs were observed in genes encoding presynaptic vesicle associated proteins, glutamate receptor subunits, and potassium channel subunits, consistent with previously reported functional differences between type I and II SGNS in glutamate responsiveness and excitability (Glowatzki and Fuchs, 2002; Grant et al., 2010; Weisz et al., 2014).

Transcriptome analyses classified the type I SGNs into 3 major subtypes, type Ia, Ib and Ic. When comparing findings across these studies, differences in the nomenclature of the subtypes must be noted. Specifically, the type Ia, Ib and Ic SGNs identified in the work by Sun et al. (2018) and Shrestha et al. (2018) refer, respectively, to the type Ic, Ia and Ib SGNs identified in the work by Petitpré et al. (2018). For clarity, the nomenclature adopted consistently in the first two studies is used here (Fig. 5B). All three studies find that the type I SGNs are approximately evenly divided between the three subtypes, with slightly more type Ia SGNs (35% to 46% of type I SGNs) and slightly fewer type Ic SGNs (25% to 34%). The three type I SGN subtypes showed little variation in their distribution between apical, middle and basal turns of the cochlea, although one study reported a slight increase in the proportion of type Ia SGNs at the expense of the type Ib SGNs (Shrestha et al., 2018). Across these studies, enriched expression of a key transcripts distinguishes subtypes, including enriched expression of *Calb2* (encoding the intracellular calcium-binding protein calbindin 2 also known as calretinin) and *Pcdh20* (encoding protocadherin 20) in type Ia SGNs, enriched expression of *Calb1* (encoding the intracellular calcium-binding protein calbindin 1) in type Ib SGNs, and enriched expression of *Pou4f1* (a transcription factor), *Lypd1* (a neurotransmitter receptor binding protein) and *Grm8* (encoding the group III metabotropic glutamate receptor 8) in the type Ic SGNs. Expression of transcripts encoding various classes of proteins important for metabolism, ion transport, morphogenesis, neurotransmission and axogenesis was enriched in the type I SGNs (Petitpré et al., 2018) and similar patterns were additionally reported by Sun et al. (2018) and Shrestha et al. (2018). Moreover, various transcripts showed subtype enrichment (Petitpré et al., 2018; Shrestha et al., 2018; Sun et al., 2018), regional (tonotopic) enrichment (Shrestha et al., 2018), and, in some cases, both subtype and regional enrichment (Shrestha et al., 2018). Importantly, classification of type I SGNs into three subtypes appears to depend on a combinatorial rather than strict on/off pattern of gene expression.

Based on their transcriptomic profiles and also projections to the IHCs, the type Ia SGNs correspond most closely to the high spontaneous rate and low threshold fibers contacting the pillar face of the IHCs. Specifically, a subpopulation of CALB2-expressing type I afferents projected preferentially to the pillar face of the IHCs (Petitpré et al., 2018; Shrestha et al., 2018; Sun et al., 2018), and decreasing CALB2-expression associated with projections preferentially more modiolar (Shrestha et al., 2018). Petitpré et al. (2018) additionally leveraged the increased expression of *Pou4f1* in the type Ic SGNs to label these neurons and trace their projections to the IHCs. Indeed, they found type Ic SGNs were *Lypd2*+, CALB2-negative and projected preferentially to the modiolar face of the IHCs. Sherrill and colleagues (2019) subsequently showed that retained expression of Pou4f1 in modiolar-targted SGNs is necessary for altered activation of presynaptic (IHC) calcium channels. Moreover, when examining SGN loss with age, a disproportionate number of type Ic SGNs were lost (Shrestha et al., 2018). This observation is consistent with previous reports of the preferential loss of SGNs with high thresholds and low spontaneous rates in gerbil (Schmiedt et al., 1996). These findings indicate that molecular expression profiles that identify subtypes of type I SGNs correlate with the previously determined distinct morphological and physiological classifications of the type I SGNs. More work is needed to establish whether subtypes of type I SGNs are distributed in gradients along the pillar-modiolar aixs (as depicted in Fig. 5B) or if, instead, they are distributed more homogenously (in a "salt-and-pepper" fashion as might be predicted from various findings regarding the organization of IHC active zones).

Finally, these three studies examined the origin of the expression profiles among the three subtypes of SGNs to gain insights into the mechanisms driving heterogeneity. In the mouse, SGNs begin forming synaptic connections with the hair cells at birth (P0), with connectivity refining over the subsequent three to four postnatal weeks (Appler and Goodrich, 2011; Bulankina and Moser, 2012; Huang et al., 2012; Macova et al., 2019; Rubel and Fritzsch, 2002). Both spontaneous activity before the onset of hearing, which begins at the start of the second postnatal week in mice (Mikaelian and Ruben, 2009), and sensory-dependent activity after the onset of hearing are believed to promote SGN specification and connectivity (Clause et al., 2014). By comparing transcript expression of SGNs isolated from mice at various postnatal ages, these three studies examined the role of postnatal activity in shaping SGN specification and came, once again, to similar conclusions. Sun et al. (2018) found comparable expression of CALB2, CALB1, POU4F1, and NGFR in all SGN types at P0. Discrete expression of type I and type II SGNs could be resolved by P7 based on restricted expression of NGFR in type II SGNs. Finally, segregation of the type I markers continued up to P28, with CALB2 enriched in type Ia SGNs, CALB1 enriched in type Ib SGNs, and POU4F1 enriched in type Ic SGNs. Similarly, Shrestha et al. (2018) found co-expression of *Calb2* (enriched in type Ia SGNs) and *Lypd1* (enriched in type Ic SGNs) in SGNs at P0.5, with segregation of these two transcripts not complete until P26. Finally, Petitpré et al. (2018) undertook a comprehensive transcriptomic approach and found that the four SGN subtypes could be identified as early as P0 (2018). Further examination of SGNs at P3 identified distinct patterns of enrichment of signaling pathways that might underly subtype specification. Together, these results indicate that the molecular specification of SGN subtypes, including signaling pathways underlying specification, are in place around birth and before the contribution of sound-evoked activity mechanisms.

Finally, Sun et al. (2018) and Shrestha et al. (2018) additionally took advantage of mouse models of congenital deafness to show that IHC activity is necessary for refinement of SGN specification. Both studies utilized VLGUT3 KO mice (Ruel et al., 2008; Seal et al., 2008), which lack the hair cell vesicular glutamate transporter, to examine the effects of abolished glutamatergic transmission between the IHCs and SGNs on the specification of type I SGNs. Both studies found that type Ic SGNs (identified as either *Lypd* + or POU4F1+ SGNs) failed to specify in these knockout mice, leading to disproportionately more type Ia and type Ib SGNs (identified as either *Calb2*+ or CALB1+/CALB2+ SGNs) (Shrestha et al., 2018; Sun et al., 2018). Sun et al. (2018) additionally examined the consequences of abolished mechanotransduction on SGN specification using mice carrying mutations in proteins essential for mechanotransduction, including *Pcdh15*, encoding a tip link protein, *Lhfpl5* and *Tmie*, both important for proper hair bundle formation. Perturbation of mechanostransduction disrupts not only specification of type I SGNs (as observed when glutamatergic signaling is disrupted) but also specification of type I and type II SGNs as indicated by increased proportion of NGFR + type II SGNs (Sun et al., 2018). Sun and colleagues additionally showed that patterns of SGN spontaneous activity were altered in mice with either disrupted mechanotransduction or glutamatergic signaling (Sun et al., 2018).

These studies provide a "transcriptional catalog" of SGN types for the genetic identification and, in the future, for genetic manipulation of specific SGN types. Indeed, a variety of transgenic mouse lines have been characterized and shown to selectively label type I or type II SGNs. These lines show expression patterns that are consistent with expectations from the three scRNAseq studies. Not necessarily predicted from the scRNseq data, however, are differences in expression observed tonotopically with some of these makers (Vyas et al., 2017, 2019; Wu et al., 2018). Specifically, *Th* and *Slc6a4* (encoding the serotonin reuptake transporter) are preferentially expressed by apical type II SGNs whereas *Calca* (encoding the calcitonin related peptide alpha) and *Drd2* (encoding the dopamine receptor D_2) are preferentially expressed by basal type II SGNs. These findings indicate mechanisms, such as additional combinatorial regulation of gene expression and/or postnatal activity, may serve to regulate tonotopic heterogeneity of SGN subtypes.

Very excitingly, this newly available transcriptomic catalog also provides a platform to identify the molecular players underlying the physical heterogeneity of the SGN subtypes. In support of this prediction and validating that transcriptomic differences in SGN subtypes are indeed associated with physiological heterogeneity, Petitpré and colleagues identified discrete accommodation rates and action potential firing patterns in genetically identified SGN type Ia/b compared to type Ic SGNs (2018), again using the SGN subtype nomenclature adopted by Sun and colleagues and Shreshta et al. (2018). The type Ia/b SGNs were identified as unitary spike accommodating (UA) SGNs whereas the type Ic SGNs were identified as multiple spike accommodating (MA) SGNs (Petitpré et al., 2018). In their work, SGNs were isolated from P21 (hearing) mice and are similar to previous findings from SGNs isolated from both prehearing (Crozier and Davis, 2014) and hearing mice (Lv et al., 2010), which classified SGNs as either rapidly or slowly adapting. This similarity despite differences in age may reflect the fact that significant transcriptomic patterning is already in place in SGNs at birth.

2.25.5 From Transcriptomic to Physiological Determinants of Afferent Neuron Heterogeneity

The task of assigning specific molecules to specific physiological properties in SGN subtypes is nevertheless still daunting. Indeed, for various reasons supported experimentally, these transcriptomic catalogs will likely not directly translate to proteomic catalogs that underlie physiological differences distinguishing SGN subtypes. First, properties of SGN subtypes will be shaped by extrinsic factors *in vivo*. Continuing with the experiments of Petitpré and colleagues investigating the physiological properties of transcriptionally identified SGN subtypes, the presumptive low threshold (high spontaneous rate) type Ia/b unitary/rapid adapting SGN subtypes had comparably higher depolarization thresholds compared to the presumptive high threshold (low spontaneous rate) type Ic multiple/slowly adapting SGNs. In other words, and perhaps not surprisingly, *in vitro* properties of SGN subtypes are not consistent with their *in vivo* properties, indicating that the molecular repertoire regulating SGN responses *in vivo* is altered during isolation and/or additionally shaped by other factors, such as IHC signaling or lateral efferent innervation (see also Section "**Lateral Efferent Innervation Modulates Afferent Neuron Activity**"). Indeed, de-efferentation causes a substantial decrease in SGN spontaneous rates *in vivo* in both cat (Liberman, 1990; Walsh et al., 1998) and chinchilla (Zheng et al., 1999) and leads to a collapse of the modiolar-pillar size gradients between presynaptic ribbons and postsynaptic glutamate receptors in mice (Yin et al., 2014). Recent work germane to the transcriptomic identification of *Pou4f1*+ type Ic SGNs showed that genetic deletion of *Pou4f1* led to small but significant changes in presynaptic voltage-gated Ca^{2+} channel activation and collapse of spatial gradients in the modiolar-pillar gradient in synaptic Ca^{2+} influx (Sherrill et al., 2019), which has been proposed to contribute presynaptically to physiological heterogeneity of type I SGNs (Ohn et al., 2016). Thus, complex mechanisms of postsynaptic regulation of presynaptic function may also underlie SGN heterogeneity.

Second, as presaged by these scRNAseq studies (Petitpré et al., 2018; Shrestha et al., 2018; Sun et al., 2018), combinatorial expression of molecules rather than expression of single molecules will likely distinguish SGN subtypes physiologically. Indeed, work performed by Liu and Davis (2014), before the availability of the SGN transcriptional catalogs, also reported the heterogenous enrichment of CALB2 (referred to as calretinin in their work) and CALB1 (referred to as calbindin in their work) in type I SGNs. Firing properties (including spike accommodation) of isolated SGNs did not, however, correlate to expression levels of either CALB2 or CALB1 alone but rather to the ratio of their expression. Third, transcript abundance does not predict protein abundance, physiological significance, or subcellular localization. For example, *Kcnc2*, encoding the fast activating $K_V3.2$ voltage-gated potassium channel, showed distinct expression patterns in subpopulations of presumptive high threshold type Ic SGNs (Petitpré

et al., 2018) and yet earlier work failed to identify KCNC2 immunofluorescently in isolated SGNs (Bakondi et al., 2008). Finally, not only expression but also subcellular localization is a critical determinant of molecular function. Voltage-gated sodium and potassium channels, for example, show very specific patterns of subcellular localization in type I SGNs *in vivo* that more than likely shape response properties of the SGNs (Kim and Rutherford, 2016).

Finally, physiological activity likely provides transcriptional feedback. For example, differences in coupling strength between the exocytosis Ca^{2+} sensor and voltage-gated Ca^{2+} channels of IHCs from base to apex have been reported recently in gerbils, with nanodomain coupling reported in the apex and middle of the cochlea and microdomain coupling reported in the base (Johnson et al., 2017). These differences in apex to basal IHC exocytosis may drive some of the observed differences in apical and basal SGN transcript expression.

Despite the complexity of utilizing transcriptomic catalogs to identify the molecular mechanisms distinguishing SGN subtypes, such catalogs are extremely powerful when applied as part of a diverse experimental toolkit. For example, recent work by Reijntjes et al. (2019) used whole transcriptomic sequencing of the isolated sensorineural structures (the organ of Corti, which contains the inner and outer hair cells, and type I and II SGNs) to obtain an inventory of molecules shaping the type I afferent signaling complex (Reijntjes and Pyott, 2016). This work particularly examined expression of transcripts encoding ion channels and identified an impressive diversity of transcripts encoding voltage-gated ion channels, and especially voltage-gated potassium ion channels, in the sensorineural structures. In fact, expression diversity rivaled that of other excitable tissues, including cerebellum and heart, indicating that a large repertoire of ion channels is positioned to determine the physiological heterogeneity of the SGNs. This observation is also consistent with scRNAseq observations in which transcripts encoding voltage-gated potassium channels (compared to voltage-gated calcium and sodium channels) showed the most substantial differences among type I SGN subtypes (Petitpré et al., 2018). Subsequent *in situ* quantitative RNA detection (using RNAscope) and patch clamp electrophysiology in isolated SGNs confirmed the expression of sodium-activated potassium channels (KCNT1 and 2) in the type I SGNs (Reijntjes et al., 2019). Auditory brainstem response measurements identified a hidden hearing loss phenotype (reduced wave I amplitudes despite normal absolute thresholds, see also Section "**Auditory Synaptopathy and Hidden Hearing Loss**") in KCNT1/2 knockout mice. This work outlined an experimental approach utilizing transcriptomic data in conjunction with mouse knockout lines and *in vitro* and *in vivo* physiology to identify the contribution of specific molecules to the physiology of SGNs and, in turn, auditory function.

2.25.6 Lateral Efferent Innervation Modulates Afferent Neuron Activity

The cochlea also receives medial and lateral innervation from the superior olivary complex in the brainstem (**Fig. 5A**). The medial lateral innervation provides inhibitory cholinergic innervation to outer hair cells and emanates from the brainstem (Vattino et al., 2020; Torres Cadenas et al., 2020). Lateral efferent inputs originate in and around the (primarily ipsilateral) lateral superior olive (Warr et al., 1997; Simmoms et al., 2011) and terminate on the type I afferent dendrites just before the spike initiation zone (Hossain et al., 2005). Moreover, lateral efferent innervation of modiolar afferents is almost twice as abundant as that of pillar afferents (Liberman, 1980, 1990; Yin et al., 2014). In cat, spontaneous firing rate correlates with the side of innervation on the inner hair cells, with high spontaneous rate fibers contacting the pillar side and low spontaneous rate fibers contacting the modiolar side (Liberman, 1982; Liberman and Oliver, 1984; Merchan-Perez and Liberman, 1996). Thus, lateral efferent innervation appears strategically positioned both to modulate excitability of the type I auditory neurons and to contribute to the heterogeneity of their response properties. Nonetheless, investigating the functional contributions of lateral efferent innervation to afferent signaling has proven challenging, and experiments examining the effects of altered lateral efferent activity—induced by either lesions, electrical stimulation, or pharmacological manipulations—reveal various and sometimes contradictory effects on afferent activity, from excitation to suppression (reviewed in Lu et al., 2016 and Reijntjes and Pyott, 2016).

Recent work (Wu et al., 2020) sheds light on not only the underlying biology of lateral efferent innervation but also the factors that may have contributed to the diversity of effects observed previously. In this work, exposure to even nontraumatic sound increased the percentage of dopaminergic lateral efferent terminals in the mouse cochlea (examined at 8 weeks of age). Dopaminergc terminals were identified by expression of the enzyme tyrosine hydroxylase, TH, necessary for the synthesis of dopamine (see also Niu and Canlon, 2002). Remarkably, these dopaminergic terminals were also cholinergic terminals arising from TH-expressing cholinergic neurons in the brainstem. Cholinergic nerve terminals and neurons were identified both genetically and immunofluorescently. Finally, this study used electrophysiological recordings of the auditory nerve fibers to show that dopamine reduces afferent firing rate presynaptically by reducing IHC release (as evidenced by overall reduced synaptic activity), but also postsynaptically by reduced EPSC amplitude and area that likely reduces AP initiation probability. The mechanisms responsible for these remarkable effects remain unknown but could presumably involve reduction of presynaptic Ca^{2+} influx and/or changes in multivesicular release. The exact mechanisms by which dopamine exerts these effects thus requires further investigations.

Importantly, this work shows that the strength of lateral efferent innervation is modulated by even non-traumatic sound exposure, involves the dynamic regulation and possible co-release of neurotransmitters, and likely utilizes both pre- and postsynaptic mechanisms. This combination of regulatory mechanisms would permit finetuning of lateral innervation and afferent sensitivity to an ever-changing acoustic environment, greatly increasing the dynamic range of afferent fibers. At the same time, such complex regulation makes disentangling the underlying mechanisms all the more challenging. Dynamic regulation of the lateral efferent input provides a new perspective from which to consider roles previously ascribed to this system, which include development

(Yin et al., 2014; reviewed in Nouvian et al., 2015), binaural balance of afferent activity (Darrow et al., 2006), and protection from acoustic injury (Darrow et al., 2007), including cochlear synaptopathy (Maison et al., 2013).

2.25.7 Additional Factors Contributing to Afferent Neuron Heterogeneity

In addition to intrinsic genetic and physiological differences in SGN subpopulations (Sections "**Transcriptomic Insights into the Determinants of Afferent Neuron Heterogeneity** and **From Transcriptomic to Physiological Determinants of Afferent Neuron Heterogeneity**) and extrinsic modulation by lateral efferent innervation (Section "**Auditory Synaptopathy and Hidden Hearing Loss**"), the molecular morphology of the afferent synapses and the spike initiation zone may also contribute to the heterogeneity of SGN afferent signaling. The morphology of the presynaptic IHC ribbons and postsynaptic glutamate receptor patches present on the type I SGNs has been proposed to contribute to shaping the response properties (spontaneous rates and spike thresholds) of SGN subpopulations (Liberman et al., 2011; Ohn et al., 2016). It turns out that the presynaptic ribbons on the modiolar side are relatively larger than those on the pillar side in many mammalian species, not only in cat (Kantardzhieva et al., 2013; Merchan-Perez and Liberman, 1996) but also mouse (Liberman et al., 2011), rat (Kalluri and Monges-Hernandez, 2017), guinea pig (Furman et al., 2013), gerbil (Zhang et al., 2018), and naked mole-rat (Barone et al., 2019). Postsynaptic glutamate receptor patches also show differences in relative size across the pillar-modiolar axis (Liberman et al., 2011), although these differences appear to vary with mouse strain (Reijntjes et al., 2020) and species (Zhang et al., 2018). These differences in synaptic morphology correspond to previous observations that the position of the synapse along the pillar-modiolar axis correlates with the spontaneous rate and threshold of the afferent fiber. Based on combined single unit recordings and retrograde labeling in cats, type I afferent fibers with low spontaneous rates and high thresholds preferentially contact the modiolar face of the IHCs, whereas fibers with high spontaneous rates and low thresholds preferentially contact the pillar face of the IHCs (Liberman, 1982). Since larger presyntpic ribbons would be expected to drive higher spontaneous rates, it is not immediately clear how the morphological configuration of the afferent synapses contributes to physiological properties of the SGNs. Thus, more anatomical, physiological, and comparative work is needed to establish the mechanisms by which volumes of synaptic proteins contribute to variations in the location and physiology of individual auditory nerve fibers and perhaps also their vulnerability to excitotoxicity (see also Section "**Auditory Synaptopathy and Hidden Hearing Loss**" below). In addition, the molecular architecture of the heminodes may also contribute to the heterogeneity of SGN response properties. The distribution of voltage gated Na^+ and K^+ channels within the spike initiation zone changes around the onset of hearing (Kim and Rutherford, 2016). Distinct patterns of developmental refinement may give rise to variations in the spontaneous rates and thresholds of SGN subpopulations.

2.25.8 Auditory Synaptopathy and Hidden Hearing Loss

Given the essential role of the afferent neurons in relaying information from the cochlea to the central auditory system, it is not surprising that dysfunction or loss of the afferent neurons causes hearing loss. More recently appreciated is that the physical or functional loss of even a small subpopulation of the synapses between the afferent neurons and sensory hair cells, in response to genetic disorders, noise exposure, or aging, can cause degraded hearing. Auditory or cochlear synaptopathy, that is the dysfunction or loss of the synapses between the type I afferent neurons and the inner hair cells, is now thought to underlie a form of auditory neuropathy (Starr et al., 1996; Moser and Starr, 2016) or hearing loss more recently dubbed hidden hearing loss (Schaette and McAlpine, 2011). Hidden hearing loss is distinguished clinically from overt hearing loss by near normal audiograms (absolute thresholds) despite complaints of hearing difficulties, especially in background noise (reviewed in Liberman, 2015; Kohrman et al., 2020). This situation in the elderly has been appreciated for decades (e.g., Saunders and Haggard, 1989) although the prevalence (of up to 15% in those between the ages of approximately 20 and 69) has only been more recently assessed and appreciated (Tremblay et al., 2015; Spankovich et al., 2018).

The biological mechanisms contributing to auditory synaptopathy and hidden hearing loss were first uncovered by experiments investigating the cochlear pathology in mice exposed to moderate noise levels (Kujawa and Liberman, 2009). In these experiments, absolute thresholds for wave I auditory brainstem responses (ABRs), which reflect the summed activity of the auditory nerve, recovered fully after noise exposure following a temporary threshold shift. However, the wave I ABR amplitudes in response to suprathreshold stimuli were reduced and failed to recovery to their pre-exposure values. Postmortem examination revealed acute loss of the inner hair cell presynaptic ribbons and retraction of postsynaptic afferent terminals. In fact, loss of auditory synapses (quantified by the loss of presynaptic ribbons) correlated to the loss of wave I ABR amplitudes, attributing pathology specifically to synaptopathy. Remarkably, loss of the auditory neuron cell bodies was substantially delayed, further attributing pathology specifically to synapse loss. Similar observations have now been documented in other mouse strains (Paquette et al., 2016), rat (Singer et al., 2013; Hickox et al., 2017), guinea pig (e.g., Lin et al., 2011), chinchilla (Hickox et al., 2017), and monkey (Valero et al., 2017). Although most experiments indicate loss of synapses is permanent, there is evidence that some degree of recovery may be possible (Shi et al., 2013; Kim et al., 2019). Similar synaptopathy has been observed in mice in response to aging (Sergeyenko et al., 2013). Finally, disrupted IHC ribbon synapse function resulting from genetic alterations can also cause auditory synaptopathy.

The loss of specific subpopulations of auditory synapses in response to noise or aging provides insight into how auditory synaptopathy might give rise hidden hearing loss. As described earlier (Section "**Afferent Fiber Heterogeneity is Essential to Relay**

Diverse Acoustic Information to the Brain"), the response properties of the type I auditory neurons distinguish at least two subgroups with either low or high spontaneous firing rates in numerous mammalian models, including rat (elBarbary, 1991), rabbit (Borg et al., 1988), cat (Liberman, 1978; Merchan-Perez and Liberman, 1996), gerbil (Schmiedt, 1989; Ohlemiller and Echteler, 1990), guinea pig (Winter et al., 1990) and different mouse strains (Taberner and Liberman, 2005). In cochlear synaptopathy, synapses associated with the auditory neurons with low spontaneous rates appear preferentially vulnerable to both noise (Furman et al., 2013) and aging (Schmiedt et al., 1996). Loss of this subpopulation of auditory neurons, which serve to expand the dynamic range of intensity coding (Schalk and Sachs, 1980), would be consistent with preservation of absolute thresholds for wave I ABRs but diminished growth of wave I ABR amplitudes in response to suprathreshold stimuli. The mechanisms underlying cochlear synaptopathy are not known, although glutamate excitotoxicity (Puel et al., 1991, 1994, 1998; Pujol et al., 1993) involving Ca^{2+}-permeable AMPA receptors is expected to play a key role (Sebe et al., 2017; Hu et al., 2020). Furthermore, cochlear synaptopathy may be caused or exacerbated by factors beyond synapse loss, including demyelination and/or disorganization of the spike initiation zone, which can lead to increased jitter in spike timing (e.g., Kim et al., 2013b; Wan and Corfas, 2017).

Identification of cochlear synaptopathy in animal models has led to reinvestigation of human temporal bone samples (Viana et al., 2015; Wu et al., 2019). The application of newer immunofluorescent techniques to identify cochlear synapses in archived tissue indicates that Schuknecht's original description of neural presbycusis (Schuknecht and Gacek, 1993) should be expanded to include not only loss of the auditory neurons but also loss of the synapses between the auditory neurons and inner hair cells, which would not have been revealed with older histological techniques. Identification of auditory assessments that can be applied clinically to diagnose cochlear synaptopathy is now an intensely active area of research (reviewed in Bharadwaj et al., 2015; Plack et al., 2016; Kohrman et al., 2020). Ultimately, the ability to prevent and/or reverse cochlear synaptopathy requires increased understanding of the underlying mechanisms, such as glutamate excitotoxicity (Sebe et al., 2017), and additional contributing factors, like altered lateral efferent innervation (see Section "**Lateral Efferent Innervation Modulates Afferent Neuron Activity**" and also Lauer et al., 2012) and myelination (see Section "**Additional Factors Contributing to Afferent Neuron Heterogeneity**"). Increasing knowledge of the genetic factors that determine physiologically defined subgroups of auditory neurons (described in Section "**Transcriptomic Insights Into the Determinants of Afferent Neuron Heterogeneity**"), should, in parallel, identify those factors that predispose subpopulations with lower spontaneous rates to increased susceptibility to noise-induced and age-related loss. Additional research also needs to be directed to identifying the mechanisms that trigger loss of the auditory neurons in response to loss of the peripheral terminals. Minimizing the extent of damage should increase the success of interventions, like cochlear implants, for restoring hearing and preserving central structure and function in response to cochlear synaptopathy (Shearer and Hansen, 2019).

2.25.9 Conclusions and Open Questions

Auditory afferents show great heterogeneity in their morphology, physiology, and patterns of protein and gene expression. Recent advances have identified molecular markers that subdivide the myelinated type I and non-myelinated type II SGNs. Remarkably, the type I SGNs can be further classified into subtypes that correspond to previously recognized electrophysiological classification of low, medium and high spontaneous rate fibers. However, despite these advances many fundamental questions remain. The developmental and activity-dependent factors that promote myelination and set the distance between the nodes of Ranvier in type I fibers during early postnatal development are still unclear. What are the factors that set the speed of action potential propagation along the fibers of the distinct type I SGNs? What are the factors that promote loss of myelination after loud sound exposure and during aging?

The type I SGN subtypes can also be functionally classified based on the sound thresholds necessary for excitation. High sound threshold (HT) axonal fibers have thin calibers, low spontaneous rates, and larger dynamic ranges. HT fiber bouton endings are also opposed to larger ribbons than low sound threshold (LT) axonal fiber bouton endings. Importantly, HT fibers are more vulnerable to damage by loud sounds and deterioration during aging. Moreover, HT fibers originating in the basal turn of the cochlea appear to be especially vulnerable, consistent with the loss of high frequency hearing in older animals and humans. Although considerable progress has been made to understand the mechanisms that distinguish the HT and LT afferent fibers, several fundamental questions persist. What are the likely distinct distributions of Na^+, K^+, HCN and Ca^{2+} channels expressed in the HT versus LT fibers (Reijntjes and Pyott, 2016)? Do these channels cluster in microdomains and, if so, where along the axon and soma of the SGNs are they located? How do they determine the threshold, refractory periods, and ability to spike at high frequencies? Why are the HT thin-caliber fibers preferentially damaged after the presentation of loud sounds or during aging? Does a low abundance of mitochondria, or perhaps high multivesicular glutamate release, or a large density of Ca^{2+}-permeable AMPA receptors, or perhaps a lower expression of Na^+/K^+-ATPase pumps play a role?

In contrast to HT fibers, do large-caliber LT fibers express a higher density of Na^+ and K^+ channels at their heminodes, which would allow for lower spike thresholds, shorter refractory periods and prolonged high-frequency spontaneous spike firing? Alternatively, can the high spontaneous rate of spikes be produced mostly by a higher spontaneous vesicle release from IHCs due to a leftward shift of voltage-dependent Ca^{2+} channel activation and a greater density of Ca^{2+} channels? Do LT axons express a larger density of Na^+/K^+-ATPase pumps and/or K^+ channels that are neuroprotective? Are they more heavily myelinated and more strongly contacted by astrocytes at their nodes of Ranvier? Is the limited dynamic range of LT fibers due to a presynaptic mechanism stemming from the smaller size of the synaptic ribbon which promotes a smaller readily releasable pool of vesicles that is quickly depleted (Kim et al., 2013a)? Or is this small dynamic range due primarily to postsynaptic mechanisms, such as enhanced Na^+

channel inactivation leading to refractoriness in high-frequency spiking or are these fibers more prone to AMPA receptor desensitization and/or saturation? Clearly, the ocean of our ignorance is vast but the recent refinements of molecular and imaging techniques provide exciting opportunities to launch new voyages of discovery.

Acknowledgements

We thank David Ryugo, Mike Muniak, Charlie Liberman and Tobias Moser for discussions and several suggestions. We also thank generous support from the National Institutes of Deafness and Communication Disorders (DC004274) and the European Research Council (764604).

References

Appler, J.M., Goodrich, L.V., 2011. Connecting the ear to the brain: molecular mechanisms of auditory circuit assembly. Prog. Neurobiol. 93 (4), 488–508.
Arnesen, A.R., Osen, K.K., 1978. The cochlear nerve in the cat: topography, cochleotopy, and fiber spectrum. J. Comp. Neurol. 178, 661–678.
Bakondi, G., Por, A., Kovacs, I., Szucs, G., Rusznak, Z., 2008. Voltage-gated K^+ channel (K_V) subunit expression of the Guinea pig spiral ganglion cells studied in a newly developed cochlear free-floating preparation. Brain Res. 1210, 148–162.
Barone, C.M., Douma, S., Reijntjes, D.O.J., Browe, B.M., Koppl, C., Klump, G., Park, T.J., Pyott, S.J., 2019. Altered cochlear innervation in developing and mature naked and Damaraland mole rats. J. Comp. Neurol. 527 (14), 2302–2316.
Berglund, A.M., Ryugo, D.K., 1991. Neurofilament antibodies and spiral ganglion neurons of the mammalian cochlea. J. Comp. Neurol. 306 (3), 393–408.
Bharadwaj, H.M., Masud, S., Mehraei, G., Verhulst, S., Shinn-Cunningham, B.G., 2015. Individual differences reveal correlates of hidden hearing deficits. J. Neurosci. 35 (5), 2161–2172.
Borg, E., Engstrom, B., Linde, G., Marklund, K., 1988. Eighth nerve fiber firing features in normal-hearing rabbits. Hear. Res. 36 (2–3), 191–201.
Bulankina, A.V., Moser, T., 2012. Neural circuit development in the mammalian cochlea. Physiology 27 (2), 100–112.
Burda, H., Branis, M., 1988. Postnatal development of the organ of Corti in the wild house mouse, laboratory mouse, and their hybrid. Hear. Res. 36, 97–105.
Chen, M., von Gersdorff, H., 2019. How to build a fast and highly sensitive sound detector that remains robust to temprature shifts. J. Neurosci. 39, 7260–7276.
Coate, T.M., Scott, M.K., Gurjar, M., 2019. Current concepts in cochlear ribbon synapse formation. Synapse 73, e22087.
Clause, A., Kim, G., Sonntag, M., Weisz, C.J., Vetter, D.E., Rubsamen, R., Kandler, K., 2014. The precise temporal pattern of prehearing spontaneous activity is necessary for tonotopic map refinement. Neuron 82 (4), 822–835.
Crozier, R.A., Davis, R.L., 2014. Unmasking of spiral ganglion neuron firing dynamics by membrane potential and neurotrophin-3. J. Neurosci. 34 (29), 9688–9702.
Darrow, K.N., Maison, S.F., Liberman, M.C., 2006. Cochlear efferent feedback balances interaural sensitivity. Nat. Neurosci. 9 (12), 1474–1476.
Darrow, K.N., Maison, S.F., Liberman, M.C., 2007. Selective removal of lateral olivocochlear efferents increases vulnerability to acute acoustic injury. J. Neurophysiol. 97 (2), 1775–1785.
El Barbary, A., 1991. Auditory nerve of the normal and jaundiced rat. I. Spontaneous discharge rate and cochlear nerve histology. Hear. Res. 54 (1), 75–90.
Friede, R.L., 1984. Cochlear axon calibres are adjusted to characteristic frequencies. J. Neurol. Sci. 66, 193–200.
Fuchs, P.A., 2018. The diversified form and function of cochlear afferents. In: Kandler, K. (Ed.), The Oxford Handbook of the Auditory Brainstem, pp. 1–26.
Furman, A.C., Kujawa, S.G., Liberman, M.C., 2013. Noise-induced cochlear neuropathy is selective for fibers with low spontaneous rates. J. Neurophysiol. 110 (3), 577–586.
Glowatzki, E., Fuchs, P.A., 2002. Transmitter release at the hair cell ribbon synapse. Nat. Neurosci. 5 (2), 147–154.
Goutman, J.D., 2012. Transmitter release from cochlear hair cells is phase locked to cyclic stimuli of different intensities and frequencies. J. Neurosci. 32, 17025–17035.
Grant, L., Yi, E., Glowatzki, E., 2010. Two modes of release shape the postsynaptic response at the inner hair cell ribbon synapse. J. Neurosci. 30 (12), 4210–4220.
Graydon, C.W., Cho, S., Li, G.L., Kachar, B., von Gersdorff, H., 2011. Sharp Ca^{2+} nanodomains beneath the ribbon promote highly synchronous multivesicular release at hair cell synapses. J. Neurosci. 31, 16637–16650.
Graydon, C.W., Cho, S., Diamond, J.S., Kachar, B., von Gersdorff, H., Grimes, W.N., 2014. Specialized postsynaptic morphology enhances neurotransmitter dilution and high-frequency signaling at an auditory synapse. J. Neurosci. 34, 8358–8372.
Grothe, B., Pecka, M., 2014. The natural history of sound localization in mammals-a story of neuronal inhibition. Front. Neural. Circ. 8, 161.
Heil, P., Peterson, A.J., 2017. Spike timing in auditory-nerve fibers during spontaneous activity and phase locking. Synapse 71, 5–36.
Hickox, A.E., Larsen, E., Heinz, M.G., Shinobu, L., Whitton, J.P., 2017. Translational issues in cochlear synaptopathy. Hear. Res. 349, 164–171.
Hossain, W.A., Antic, S.D., Yang, Y., Rasband, M.N., Morest, D.K., 2005. Where is the spike generator of the cochlear nerve? Voltage-gated sodium channels in the mouse cochlea. J. Neurosci. 25 (29), 6857–6868.
Hu, N., Rutherford, M.A., Green, S.H., 2020. Protection of cochlear synapses from noise-induced excitotoxic trauma by blockade of Ca^{2+}-permeable AMPA receptors. Proc. Natl. Acad. Sci. U. S. A. 117 (7), 3828–3838.
Huang, L.C., Barclay, M., Lee, K., Peter, S., Housley, G.D., Thorne, P.R., Montgomery, J.M., 2012. Synaptic profiles during neurite extension, refinement and retraction in the developing cochlea. Neural Dev. 7, 38.
Johnson, S.L., Olt, J., Cho, S., von Gersdorff, H., Marcotti, W., 2017. The coupling between Ca^{2+} channels and the exocytotic Ca^{2+} sensor at hair cell ribbon synapses varies tonotopically along the mature cochlea. J. Neurosci. 37 (9), 2471–2484.
Kalluri, R., Monges-Hernandez, M., 2017. Spatial gradients in the size of inner hair cell ribbons emerge before the onset of hearing in rats. J. Assoc. Res. Otolaryngol. 18 (3), 399–413.
Kantardzhieva, A., Liberman, M.C., Sewell, W.F., 2013. Quantitative analysis of ribbons, vesicles, and cisterns at the cat inner hair cell synapse: correlations with spontaneous rate. J. Comp. Neurol. 521, 3260–3271.
Kim, M.H., Li, G.L., von Gersdorff, H., 2013a. Single Ca^{2+} channels and exocytosis at sensory synapses. J. Physiol. 591, 3167–3178.
Kim, J.H., Renden, R., von Gersdorff, H., 2013b. Dysmyelination of auditory afferent axons increases the jitter of action potential timing during high-frequency firing. J. Neurosci. 33, 9402–9407.
Kim, K.X., Payne, S., Yang-Hood, A., Li, S.Z., Davis, B., Carlquist, J., V-Ghaffari, B., Gantz, J.A., Kallogjeri, D., Fitzpatrick, J.A.J., Ohlemiller, K.K., Hirose, K., Rutherford, M.A., 2019. Vesicular glutamatergic transmission in noise-induced loss and repair of cochlear ribbon synapses. J. Neurosci. 39, 4434–4447.
Kim, K.X., Rutherford, M.A., 2016. Maturation of Na_V and K_V channel topographies in the auditory nerve spike initiator before and after developmental onset of hearing function. J. Neurosci. 36, 2111–2118.
Kohrman, D.C., Wan, G., Cassinotti, L., Corfas, G., 2020. Hidden hearing loss: a disorder with multiple etiologies and mechanisms. Cold Spring Harb. Perspect Med. 10 (1).
Kujawa, S.G., Liberman, M.C., 2009. Adding insult to injury: cochlear nerve degeneration after "temporary" noise-induced hearing loss. J. Neurosci. 29, 14077–14085.
Lauer, A.M., Fuchs, P.A., Ryugo, D.K., Francis, H.W., 2012. Efferent synapses return to inner hair cells in the aging cochlea. Neurobiol. Aging 33, 2892–2902.

Li, G.L., Keen, E., Andor-Ardó, D., Hudspeth, A.J., von Gersdorff, H., 2009. The unitary event underlying multiquantal EPSCs at a hair cell's ribbon synapse. J. Neurosci. 29, 7558–7568.
Li, G.L., Cho, S., von Gersdorff, H., 2014. Phase-locking precision is enhanced by multiquantal release at an auditory hair cell ribbon synapse. Neuron 83, 1404–1417.
Li, C., Li, X., Bi, Z., Sugino, K., Wang, G., Zhu, T., Liu, Z., 2020. Comprehensive transcriptome analysis of cochlear spiral ganglion neurons at multiple ages. Elife 9.
Liberman, L.D., Wang, H., Liberman, M.C., 2011. Opposing gradients of ribbon size and AMPA receptor expression underlie sensitivity differences among cochlear-nerve/hair-cell synapses. J. Neurosci. 31, 801–808.
Liberman, M.C., 1978. Auditory-nerve response from cats raised in a low-noise chamber. J. Acoust. Soc. Am. 63 (2), 442–455.
Liberman, M.C., 1980. Efferent synapses in the inner hair cell area of the cat cochlea: an electron microscopic study of serial sections. Hear. Res. 3 (3), 189–204.
Liberman, M.C., 1982. Single-neuron labeling in the cat auditory nerve. Science 216 (4551), 1239–1241.
Liberman, M.C., 1990. Effects of chronic cochlear de-efferentation on auditory-nerve response. Hear. Res. 49 (1–3), 209–223.
Liberman, M.C., 2015. Hidden hearing loss. Sci. Am. 313 (2), 48–53.
Liberman, M.C., 2017. Noise-induced and age-related hearing loss: new perspectives and potential therapies. F1000Res. 6, 927.
Liberman, M.C., Oliver, M.E., 1984. Morphometry of intracellularly labeled neurons of the auditory nerve: correlations with functional properties. J. Comp. Neurol. 223 (2), 163–176.
Lin, H.W., Furman, A.C., Kujawa, S.G., Liberman, M.C., 2011. Primary neural degeneration in the Guinea pig cochlea after reversible noise-induced threshold shift. J. Assoc. Res. Otolaryngol. 12 (5), 605–616.
Liu, W., Davis, R.L., 2014. Calretinin and calbindin distribution patterns specify subpopulations of type I and type II spiral ganglion neurons in postnatal murine cochlea. J. Comp. Neurol. 522 (10), 2299–2318.
Lu, X., Shu, Y., Tang, M., Li, H., 2016. Mammalian cochlear hair cell regeneration and ribbon synapse reformation. Neural Plast. 2016, 1–9.
Lv, P., Wei, D., Yamoah, E.N., 2010. Kv7-type channel currents in spiral ganglion neurons: involvement in sensorineural hearing loss. J. Biol. Chem. 285 (45), 34699–34707.
Macova, I., Pysanenko, K., Chumak, T., Dvorakova, M., Bohuslavova, R., Syka, J., Fritzsch, B., Pavlinkova, G., 2019. Neurod1 is essential for the primary tonotopic organization and related auditory information processing in the midbrain. J. Neurosci. 39, 984–1004.
Maison, S.F., Usubuchi, H., Liberman, M.C., 2013. Efferent feedback minimizes cochlear neuropathy from moderate noise exposure. J. Neurosci. 33 (13), 5542–5552.
McLean, W.J., Smith, K.A., Glowatzki, E., Pyott, 2009. Distribution of the Na/K-ATPase alpha subunit in the rat spiral ganglion and organ of Corti. J. Assoc. Res. Otolaryngol. 10, 37–49.
Merchan-Perez, A., Liberman, M.C., 1996. Ultrastructural differences among afferent synapses on cochlear hair cells: correlations with spontaneous discharge rate. J. Comp. Neurol. 371 (2), 208–221.
Mikaelian, D., Ruben, R., 2009. Development of hearing in the normal cba-J mouse: correlation of physiological observations with behavioral responses and with cochlear anatomy. Acta Otolaryngol. 59, 451–461.
Moser, T., Grabner, C.P., Schmitz, F., 2020. Sensory Processing at Ribbon Synapses in the Retina and the Cochlea. Physiol. Rev. 100, 103–144.
Moser, T., Starr, A., 2016. Auditory neuropathy–neural and synaptic mechanisms. Nat. Rev. Neurol. 12, 135–149.
Muniak, M.A., Connelly, C.J., Suthakar, K., Milinkeviciute, G., Ayeni, F.E., Ryugo, D.K., 2016. Central projections of spiral ganglion neurons. In: The Primary Auditory Neurons of the Mammalian Cochlea, vol. 52. Springer, New York, NY, pp. 157–190.
Niu, X., Canlon, B., 2002. Activation of tyrosine hydroxylase in the lateral efferent terminals by sound conditioning. Hear. Res. 174 (1–2), 124–132.
Nouvian, R., Eybalin, M., Puel, J.L., 2015. Cochlear efferents in developing adult and pathological conditions. Cell Tissue Res. 361 (1), 301–309.
Ohlemiller, K.K., Echteler, S.M., 1990. Functional correlates of characteristic frequency in single cochlear nerve fibers of the Mongolian gerbil. J. Comp. Physiol. 167 (3), 329–338.
Ohn, T.L., Rutherford, M.A., Jing, Z., Jung, S., Duque-Afonso, C.J., Hoch, G., Picher, M.M., Scharinger, A., Strenzke, N., Moser, T., 2016. Hair cells use active zones with different voltage dependence of Ca^{2+} influx to decompose sounds into complementary neural codes. Proc. Natl. Acad. Sci. U. S. A. 113 (32), E4716–E4725.
Paquette, S.T., Gilels, F., White, P.M., 2016. Noise exposure modulates cochlear inner hair cell ribbon volumes, correlating with changes in auditory measures in the FVB/nJ mouse. Sci. Rep. 6, 25056.
Petitpré, C., Wu, H., Sharma, A., Tokarska, A., Fontanet, P., Wang, Y., Helmbacher, F., Yackle, K., Silberberg, G., Hadjab, S., Lallemend, F., 2018. Neuronal heterogeneity and stereotyped connectivity in the auditory afferent system. Nat. Commun. 9 (1), 3691.
Plack, C.J., Leger, A., Prendergast, G., Kluk, K., Guest, H., Munro, K.J., 2016. Toward a diagnostic test for hidden hearing loss. Trends Hear. 20.
Puel, J.L., Pujol, R., Ladrech, S., Eybalin, M., 1991. Alpha-amino-3-hydroxy-5-methyl-4-isoxazole propionic acid electrophysiological and neurotoxic effects in the Guinea-pig cochlea. Neuroscience 45 (1), 63–72.
Puel, J.L., Pujol, R., Tribillac, F., Ladrech, S., Eybalin, M., 1994. Excitatory amino acid antagonists protect cochlear auditory neurons from excitotoxicity. J. Comp. Neurol. 341 (2), 241–256.
Puel, J.L., Ruel, J., Gervais d'Aldin, C., Pujol, R., 1998. Excitotoxicity and repair of cochlear synapses after noise-trauma induced hearing loss. Neuroreport 9 (9), 2109–2114.
Pujol, R., Puel, J.L., Gervais d'Aldin, C., Eybalin, M., 1993. Pathophysiology of the glutamatergic synapses in the cochlea. Acta Otolaryngol. 113 (3), 330–334.
Reijntjes, D.O.J., Koppl, C., Pyott, S.J., 2020. Volume gradients in inner hair cell-auditory nerve fiber pre- and postsynaptic proteins differ across mouse strains. Hear. Res. 390, 107933.
Reijntjes, D.O.J., Lee, J.H., Park, S., Schubert, N.M.A., van Tuinen, M., Vijayakumar, S., Jones, T.A., Jones, S.M., Gratton, M.A., Xia, X.M., Yamoah, E.N., Pyott, S.J., 2019. Sodium-activated potassium channels shape peripheral auditory function and activity of the primary auditory neurons in mice. Sci. Rep. 9 (1), 2573.
Reijntjes, D.O.J., Pyott, S.J., 2016. The afferent signaling complex: regulation of type I spiral ganglion neuron responses in the auditory periphery. Hear. Res. 336, 1–16.
Risoud, M., Sircoglou, J., Dedieu, G., Tardivel, M., Vincent, C., Bonne, N.-X., 2017. Imaging and cell count in cleared intact cochlea in the Mongolian gerbil using laser scanning confocal microscopy. Eur. Ann. Otorhinolaryngol. Head. Neck. Dis. 134, 221–224.
Rodriguez-Contreras, A., Yamoah, E.N., 2001. Direct measurement of single-channel Ca^{2+} currents in bullfrog hair cells reveals two distinct channel subtypes. J. Physiol. 534, 669–689.
Rose, J.E., Brugge, J.F., Anderson, D.J., Hind, J.E., 1967. Phase-locked response to low-frequency tones in single auditory nerve fibers of the squirrel monkey. J. Neurophysiol. 30, 769–793.
Rubel, E.W., Fritzsch, B., 2002. Auditory system development: primary auditory neurons and their targets. Annu. Rev. Neurosci. 25, 51–101.
Ruel, J., Emery, S., Nouvian, R., Bersot, T., Amilhon, B., Van Rybroek, J.M., Rebillard, G., Lenoir, M., Eybalin, M., Delprat, B., Sivakumaran, T.A., Giros, B., El Mestikawy, S., Moser, T., Smith, R.J., Lesperance, M.M., Puel, J.L., 2008. Impairment of SLC17A8 encoding vesicular glutamate transporter-3, VGLUT3, underlies nonsyndromic deafness DFNA25 and inner hair cell dysfunction in null mice. Am. J. Hum. Genet. 83 (2), 278–292.
Rutherford, M.A., 2015. Resolving the structure of the inner ear ribbon synapses with STED microscopy. Synapse 69, 242–255.
Rutherford, M.A., Chapochnikov, N.M., Moser, T., 2012. Spike encoding of neurotransmitter release timing by spiral ganglion neurons of the cochlea. J. Neurosci. 32, 4773–4789.
Rutherford, M.A., Moser, T., 2016. The ribbon synapse between type I spiral ganglion neurons and inner hair cells. In: Dabdoub, A., Fritzsch, B. (Eds.), Springer Handbook of Auditory Research, vol. 52, pp. 117–156.
Saunders, G.H., Haggard, M.P., 1989. The clinical assessment of obscure auditory dysfunction–1. Auditory and psychological factors. Ear Hear. 10 (3), 200–208.
Schaette, R., McAlpine, D., 2011. Tinnitus with a normal audiogram: physiological evidence for hidden hearing loss and computational model. J. Neurosci. 31 (38), 13452–13457.
Schalk, T.B., Sachs, M.B., 1980. Nonlinearities in auditory-nerve fiber responses to bandlimited noise. J. Acoust. Soc. Am. 67 (3), 903–913.
Schmiedt, R.A., 1989. Spontaneous rates, thresholds and tuning of auditory-nerve fibers in the gerbil: comparisons to cat data. Hear. Res. 42 (1), 23–35.
Schmiedt, R.A., Mills, J.H., Boettcher, F.A., 1996. Age-related loss of activity of auditory-nerve fibers. J. Neurophysiol. 76 (4), 2799–2803.
Schuknecht, H.F., Gacek, M.R., 1993. Cochlear pathology in presbycusis. Ann. Otol. Rhinol. Laryngol. 102 (1 Pt 2), 1–16.

Schnee, M.E., Castellano-Muñoz, M., Ricci, A.J., 2013. Response properties from turtle auditory hair cell afferent fibers suggest spike generation is driven by synchronized release both between and within synapses. J. Neurophysiol. 110, 204–220.
Seal, R.P., Akil, O., Yi, E., Weber, C.M., Grant, L., Yoo, J., Clause, A., Kandler, K., Noebels, J.L., Glowatzki, E., Lustig, L.R., Edwards, R.H., 2008. Sensorineural deafness and seizures in mice lacking vesicular glutamate transporter 3. Neuron 57 (2), 263–275.
Sebe, J.Y., Cho, S., Sheets, L., Rutherford, M.A., von Gersdorff, H., Raible, D.W., 2017. Ca^{2+}-permeable AMPARs mediate glutamatergic transmission and excitotoxic damage at the hair cell ribbon synapse. J. Neurosci. 37 (25), 6162–6175.
Sergeyenko, Y., Lall, K., Liberman, M.C., Kujawa, S.G., 2013. Age-related cochlear synaptopathy: an early-onset contributor to auditory functional decline. J. Neurosci. 33 (34), 13686–13694.
Shearer, A.E., Hansen, M.R., 2019. Auditory synaptopathy, auditory neuropathy, and cochlear implantation. Laryngoscope Investig. Otolaryngol. 4 (4), 429–440.
Sherrill, H.E., Jean, P., Driver, E.C., Sanders, T.R., Fitzgerald, T.S., Moser, T., Kelley, M.W., 2019. Pou4f1 defines a subgroup of type I spiral ganglion neurons and is necessary for normal inner hair cell presynaptic Ca(2+) signaling. J. Neurosci. 39 (27), 5284–5298.
Shi, L., Liu, L., He, T., Guo, X., Yu, Z., Yin, S., Wang, J., 2013. Ribbon synapse plasticity in the cochleae of Guinea pigs after noise-induced silent damage. PloS One 8 (12), e81566.
Shrestha, B.R., Chia, C., Wu, L., Kujawa, S.G., Liberman, M.C., Goodrich, L.V., 2018. Sensory neuron diversity in the inner ear is shaped by activity. Cell 174 (5), 1229–1246.e1217.
Simmons, D., Duncan, J., de Caprona, D.C., Fritzsch, B., 2011. Development of the inner ear efferent system. In: Auditory and Vestibular Efferents. Springer, New York, NY, pp. 187–216.
Singer, W., Zuccotti, A., Jaumann, M., Lee, S.C., Panford-Walsh, R., Xiong, H., Zimmermann, U., Franz, C., Geisler, H.S., Kopschall, I., Rohbock, K., Varakina, K., Verpoorten, S., Reinbothe, T., Schimmang, T., Ruttiger, L., Knipper, M., 2013. Noise-induced inner hair cell ribbon loss disturbs central arc mobilization: a novel molecular paradigm for understanding tinnitus. Mol. Neurobiol. 47 (1), 261–279.
Spankovich, C., Gonzalez, V.B., Su, D., Bishop, C.E., 2018. Self reported hearing difficulty, tinnitus, and normal audiometric thresholds, the National Health and Nutrition Examination Survey 1999-2002. Hear. Res. 358, 30–36.
Spoendlin, H., 1969. Innervation patterns in the organ of Corti of the cat. Acta Otolaryngol. 67, 239–254.
Starr, A., Picton, T.W., Sininger, Y., Hood, L.J., Berlin, C.I., 1996. Auditory neuropathy. Brain 119 (Pt 3), 741–753.
Sun, S., Babola, T., Pregernig, G., So, K.S., Nguyen, M., Su, S.M., Palermo, A.T., Bergles, D.E., Burns, J.C., Muller, U., 2018. Hair cell mechanotransduction regulates spontaneous activity and spiral ganglion subtype specification in the auditory system. Cell 174 (5), 1247–1263. e1215.
Taberner, A.M., Liberman, M.C., 2005. Response properties of single auditory nerve fibers in the mouse. J. Neurophysiol. 93 (1), 557–569.
Torres Cadenas, L., Fischl, M.J., Weisz, C.J.C., 2020. Synaptic inhibition of medial olivocochlear efferent neurons by neurons of the medial nucleus of the trapezoid body. J. Neurosci. 40, 509–525.
Tsuji, J., Liberman, M.C., 1997. Intracellular labeling of auditory nerve fibers in Guinea pig: central and peripheral projections. J. Comp. Neurol. 381, 188–202.
Tremblay, K.L., Pinto, A., Fischer, M.E., Klein, B.E., Klein, R., Levy, S., Tweed, T.S., Cruickshanks, K.J., 2015. Self-reported hearing difficulties among adults with normal audiograms: the beaver dam offspring study. Ear Hear. 36 (6), e290–299.
Valero, M.D., Burton, J.A., Hauser, S.N., Hackett, T.A., Ramachandran, R., Liberman, M.C., 2017. Noise-induced cochlear synaptopathy in rhesus monkeys (*Macaca mulatta*). Hear. Res. 353, 213–223.
Vattino, L.G., Wedemeyer, C., Elgoyhen, A.B., Katz, E., 2020. Functional postnatal maturation of the medial olivocochlear efferent-outer hair cell synapse. J. Neurosci. 40, 4842–4857.
Viana, L.M., O'Malley, J.T., Burgess, B.J., Jones, D.D., Oliveira, C.A., Santos, F., Merchant, S.N., Liberman, L.D., Liberman, M.C., 2015. Cochlear neuropathy in human presbycusis: confocal analysis of hidden hearing loss in post-mortem tissue. Hear. Res. 327, 78–88.
Vyas, P., Wu, J.S., Jimenez, A., Glowatzki, E., Fuchs, P.A., 2019. Characterization of transgenic mouse lines for labeling type I and type II afferent neurons in the cochlea. Sci. Rep. 9 (1), 5549.
Vyas, P., Wu, J.S., Zimmerman, A., Fuchs, P., Glowatzki, E., 2017. Tyrosine hydroxylase expression in type II cochlear afferents in mice. J. Assoc. Res. Otolaryngol. 18 (1), 139–151.
Walsh, E.J., McGee, J., McFadden, S.L., Liberman, M.C., 1998. Long-term effects of sectioning the olivocochlear bundle in neonatal cats. J. Neurosci. 18 (10), 3859–3869.
Wan, G., Corfas, G., 2017. Transient auditory nerve demyelination as a new mechanism for hidden hearing loss. Nat. Commun. 8, 14487.
Warr, W.B., Boche, J.B., Neely, S.T., 1997. Efferent innervation of the inner hair cell region: origins and terminations of two lateral olivocochlear systems. Hear. Res. 108 (1–2), 89–111.
Weisz, C.J., Glowatzki, E., Fuchs, P.A., 2014. Excitability of type II cochlear afferents. J. Neurosci. 34 (6), 2365–2373.
Wittig Jr., J.H., Parsons, T.D., 2008. Synaptic ribbon enables temporal precision of hair cellafferent synapse by increasing the number of readily releasable vesicles: a modeling study. J. Neurophysiol. 100, 1724–1739.
Winter, I.M., Robertson, D., Yates, G.K., 1990. Diversity of characteristic frequency rate-intensity functions in Guinea pig auditory nerve fibres. Hear. Res. 45 (3), 191–202.
Wu, J.S., Young, E.D., Glowatzki, E., 2016. Maturation of spontaneous riring properties after hearing onset in rat auditory nerve fibers: spontaneous rates, refractoriness, and interfiber correlations. J. Neurosci. 36, 10584–10597.
Wu, J.S., Vyas, P., Glowatzki, E., Fuchs, P.A., 2018. Opposing expression gradients of calcitonin-related polypeptide alpha (Calca/Cgrpalpha) and tyrosine hydroxylase (Th) in type II afferent neurons of the mouse cochlea. J. Comp. Neurol. 526 (3), 425–438.
Wu, J.S., Yi, E., Manca, M., Javaid, H., Lauer, A.M., Glowatzki, E., 2020. Sound exposure dynamically induces dopamine synthesis in cholinergic LOC efferents for feedback to auditory nerve fibers. Elife 9.
Wu, P.Z., Liberman, L.D., Bennett, K., de Gruttola, V., O'Malley, J.T., Liberman, M.C., 2019. Primary neural degeneration in the human cochlea: evidence for hidden hearing loss in the aging ear. Neuroscience 407, 8–20.
Yin, Y., Liberman, L.D., Maison, S.F., Liberman, M.C., 2014. Olivocochlear innervation maintains the normal modiolar-pillar and habenular-cuticular gradients in cochlear synaptic morphology. J. Assoc. Res. Otolaryngol. 15 (4), 571–583.
Zampini, V., Johnson, S.L., Franz, C., Lawrence, N.D., Münkner, S., Engel, J., Knipper, M., Magistretti, J., Masetto, S., Marcotti, W., 2010. Elementary properties of $Ca_V1.3$ Ca^{2+} channels expressed in mouse cochlear inner hair cells. J. Physiol. 588, 187–199.
Zhang, L., Engler, S., Koepcke, L., Steenken, F., Koppl, C., 2018. Concurrent gradients of ribbon volume and AMPA-receptor patch volume in cochlear afferent synapses on gerbil inner hair cells. Hear. Res. 364, 81–89.
Zheng, X.Y., Henderson, D., McFadden, S.L., Ding, D.L., Salvi, R.J., 1999. Auditory nerve fiber responses following chronic cochlear de-efferentation. J. Comp. Neurol. 406 (1), 72–86.